Footprint Model in a Navigation System Based on Visible Light Communication

Paula Louro, Manuela Vieira, Manuel Augusto Vieira
DEETC/ISEL/IPL,
R. Conselheiro Emídio Navarro, 1959-007
Lisboa, Portugal
CTS-UNINOVA
Quinta da Torre, Monte da Caparica, 2829-516,
Caparica, Portugal
e-mail: plouro@deetc.isel.pt, mv@isel.ipl.pt,
mvieira@deetc.isel.pt

Mirtes de Lima, João Rodrigues, Pedro Vieira
DEETC/ISEL/IPL,
R. Conselheiro Emídio Navarro, 1959-007
Lisboa, Portugal
Instituto das Telecomunicações
Instituto Superior Técnico, 1049-001,
Lisboa, Portugal
e-mail: A43891@alunos.isel.pt; A42101@alunos.isel.pt,
pedro.vieira@isel.pt

***Abstract*— Indoor navigation is hardly managed by the usual Global Positioning System (GPS) due to the strong attenuation of signals inside the buildings. Alternative based on RF optical, magnetic or acoustic signals can be used. Among the optical technologies, Visible Light Communication (VLC) provides good position accuracy. The proposed system uses commercial RGB white LEDs for the generation of the light, which is simultaneously coded and modulated to transmit information. The receiver includes a multilayered photodetector based on a-SiC:H operating in the visible spectrum. The positioning system includes multiple, identical navigation cells. Inside each cell, the optical pattern defined by the VLC transmitters establishes specific spatial regions assigned each to different optical excitations, which configures the footprint of the navigation cell. Demodulation and decoding procedures of the photocurrent signal measured by the photodetector are used to identify the input optical excitations and enable position recognition inside the cell. The footprint model is characterized using geometrical and optical assumptions, namely the Lambertian model for the LEDs and the evaluation of the channel gain of the VLC link. An algorithm to decode the information is established and the positioning accuracy is discussed. The experimental results confirmed that the proposed VLC architecture is suitable for the intended application.**

Keywords- Visible Light Communication; Indoor navigation; White LEDs; Lambertian model; navigation cell.

I. INTRODUCTION

Indoor positioning can be addressed by several techniques, such as Wi-Fi, Assisted GPS (A-GPS), Infrared, Radio Frequency Identification (RFID), and many other technologies [1][2]. The ubiquitous presence of indoor Light Emitting Diodes (LED) based lighting systems enabled Visible Light communication (VLC) as an attractive technology to perform such task. Furthermore, enhanced accuracy is an additional added value to this solution. VLC is a technology based on the use of visible light in the THz range, extending from 400 nm up to 750 nm [3][4]. VLC systems use modulated LEDs to transmit information taking advantage of ubiquitous, energy efficient white LED infra-structures, designed primarily for lighting purposes [5]. Due to its characteristics, LEDs [6] can be switched very fast to produce modulated light in high frequencies, allowing data transmission in high speed. Consequently, this free-space, wireless optical communication technology is attractive to address the growing need for energy saving and speed network data transmission [7][8]. As the technology is mainly related to energy saving lighting sources it uses mostly white LEDs [9][10], either based on blue emitter coated with a phosphor layer or based on tri-chromatic emitters. The phosphor-based LED typically consists of a blue LED chip covered by a yellow phosphor layer. However, when this phosphor-based LED is used for VLC, the modulation bandwidth is limited by the long relaxation time of the phosphor; hence limiting the transmission capacity of the VLC. The increase of the LED modulation bandwidth, can be achieved using a blue filter before the receiver unit to eliminate the slow-response of the yellow light component [11][12]. The tri-chromatic LEDs are more expensive but provide additional bandwidth as three communication channels can be used by independent modulation of each chip of the monolithic device.

The receiver unit of VLC systems usually include based silicon photodiodes, as these devices operate in the visible region of the spectrum. Several applications of VLC systems are currently being developed, spanning from low data rate applications such as indoor positioning and navigation to more demanding bandwidth applications like multimedia streaming or internet access points [13][14].
In this paper we propose the use of a multilayered a:SiC:H [15] device to perform the photodetection of the optical signals generated by white trichromatic RGB LEDs [16], [17]. The system was designed for navigation [18][19], and the emitters of each white LED were specifically modulated at precise frequencies and coding bit sequences [20][21].

The proposed lighting and positioning/navigation system involves wireless communication, computer based algorithms, smart sensor and optical sources network, which

 ISBN: 978-1-61208-918-8

constitutes a transdisciplinary approach framed in cyber-physical systems.

The paper is organized as follows. After the introduction (Section I), the VLC system architecture is presented in Section II. In Section III, models for the footprint characterization using both geometrical and propagation assumptions are analyzed. In Section IV, the communication protocol and the encoding/decoding techniques are analyzed and discussed. At last, conclusions are addressed in Section V.

II. VLC SYSTEM ARCHITECTURE

In the proposed VLC system, the transmitter is composed of white RGB LEDs that code the information and modulate the emitted light and of a receiver with a photodiode that measures the modulated signal from the transmitted light and decodes information through a dedicated algorithm for data analysis. The transmitter and the receiver are physically separated from each other, but connected through the VLC channel. In this solution we work in line of sight conditions using the atmosphere as transmission channel.

A. VLC Transmitter

The transmitter proposed in this VLC system uses ceiling lamps based on commercial white LEDs. with red, green and blue emitters (w-RGB LEDs). Each ceiling lamp is composed of four white LEDs framed at the corners of a square (Figure 1).

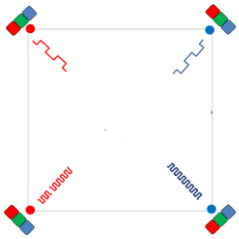

Figure 1. Configuration of the VLC emitter with 4 RGB white LEDs.

The luminous intensity of each emitter is regulated by the driving current for white perception by the human eye and the divergence angle is around 120º.

On each corner only one chip of each white LED is modulated for data transmission carrying useful information. The other emitters of the LED are only supplied with DC to maintain white color illumination. Red (R; 626 nm), Green (G; 530 nm), Blue (B; 470 nm) and violet (V; 390 nm) LEDs, are used [22].

B. VLC Receiver

The receiver is a pinpin photodiode that transduces the light into an electrical signal able to be demodulated and decoded. This device is a monolithic heterojunction composed of two pin structures based on a-Si:H and a-SiC:H built on a glass substrate and sandwiched between two transparent electrical contacts. The intrinsic absorber materials of both pin structures of the photodiode were designed to enable separate detection of short and long visible wavelengths. The front, thin pin structure made of a-SiC:H exhibits high absorption to short wavelengths (blue, and green light in this case) and high transparency to the long wavelength (red light). In opposition, the back, thicker pin structure based on a-Si:H absorbs only long wavelengths (green and red). The device selectivity is tuned externally using reverse bias (-8 V) and optical steady state illumination of short wavelength (400 nm).

III. FOOTPRINT, ARCHITECTURE AND BUILDING MODEL

The lamp configuration at the ceiling constitutes a basic unit illumination infrastructure and defines a communication cell, which coverage will be discussed in next sections.

A. Footprint definition and geometrical characterization

Each lamp with this configuration constitutes a navigation unit cell) inside which the coverage of the modulated light allows the characterization of different spatial regions assigned to specific illumination patterns. This provides higher accuracy inside the cell for the position determination, and enables the concept of footprint inside the navigation cell (Figure 2). To provide wider illumination and communication signal coverage, several VLC emitters must be placed in adjacent positions, defining thus adjacent, independent navigation cells. To provide wider illumination and communication signal coverage, several VLC emitters must be placed in adjacent positions, defining thus adjacent, independent navigation cells.

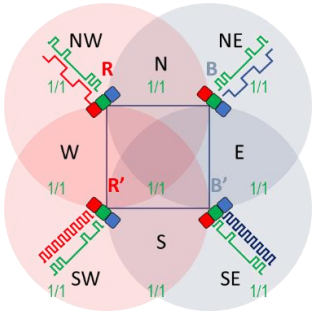

Figure 2. Configuration of the unit navigation cell.

In this model, we will assume that each white LED cone of light overlaps in the central region of the square. In the lateral and corner parts, this intersection is partial due to the radiation patterns superposition of the closest two or three LEDs [23]. Outside the square, distinct optical regions correspond also to different spatial regions, with the presence of a single red or blue signal or of two signals (red and blue, or two red or two blue signals). Consequently, the area covered by the different optical excitations will vary along the navigation unit cell (Figure 3).

 ISBN: 978-1-61208-918-8

The central region, labeled β results from the overlap of the emitted light from the two red emitters, two blue emitters and four green emitters, while the α region at the corners holds the optical excitation of three green emitters and two blue and one red, or two red and one blue emitter. At the γ and γ' regions the optical pattern is due to two emitters (two green emitters and two blue or two red emitters or one red and one blue emitter). Regions δ and Δ include the irradiation pattern from one single white-LED, i.e., light from one green emitter and from one red or blue emitter. Regions of the navigation cell not covered by any irradiation pattern, correspond to "dark" regions, where the photodetector will not be able the perceive the position.

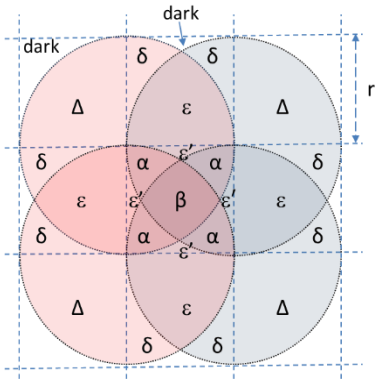

Figure 3. Diagram of the radiation patterns within each navigation unit cell.

As can be depicted from Figure 3, the area covered by each irradiation pattern can be evaluated using simple geometrical considerations. This was computed integrating the shadowed area of each region, assuming a circular irradiation flux for each emitter of radius r.

Thus,

$$A_\varepsilon = 2 \times \int_{r/2}^{r} \sqrt{r^2 - x^2} \cdot dx \quad (1)$$

$$A_\beta = 4\left[\int_{r/2}^{\sqrt{3}r/2} \sqrt{r^2 - x^2} dx - r^2\left(\frac{\sqrt{3}}{2} - \frac{1}{2}\right)^2\right] \quad (2)$$

Using polar coordinates equations (1) and (2) can be written as:

$$A_\varepsilon = 2 \times \int_{0}^{\pi/3} r^2 \sin^2\theta \cdot d\theta \quad (3)$$

$$A_\beta = 4\left(\int_{\pi/6}^{\pi/3} r^2 sin^2\theta \cdot d\theta + r^2\left(1 - \frac{\sqrt{3}}{2}\right)\right) \quad (4)$$

The solution of equations (3) and (4) is:

$$A_\varepsilon = r^2\left(\frac{\pi}{3} - \frac{\sqrt{3}}{4}\right) \quad (5)$$

$$A_\beta = r^2\left(\frac{\pi}{12} - 1 + \frac{\sqrt{3}}{2}\right) = 0.315147 \cdot r^2 \quad (6)$$

The evaluation of adjacent areas is given by:

$$A_\delta = \frac{\pi r^2}{4} - A_\varepsilon = 0.171213 \cdot r^2 \quad (7)$$

$$A_{\varepsilon'} = r^2 - A_\varepsilon - 2 \cdot A_\delta = 0.043389 \cdot r^2 \quad (8)$$

$$A_\alpha = \frac{1}{4}\left(r^2 - A_\beta - 4 \times A_{\varepsilon'}\right) = 0.337418 r^2 \quad (9)$$

Table I summarizes the numerical values of the normalized area of each footprint inside the navigation cell inside (assuming an area 3r×3r for the navigation unit cell).

TABLE I. RELATIVE AREA OF THE IRRADIATION PATTERNS WITHIN THE NAVIGATION UNIT CELL.

Spatial region	Area	Number of regions	Normalized area (navigation unit cell)
ε	0,614·r²	4	0,273
δ	0,171·r²	8	0,152
ε'	0,043·r²	4	0,019
β	0,511·r²	1	0,057
α	0,079·r²	4	0,035
Δ	0,785·r²	4	0,349
Δ+ δ	0,957·r²	4	0,501
ε + ε'	0,658·r²	4	0,292
Dark	0,215·r²	4	0,095

These values allow the evaluation of the accuracy on the determination on the spatial resolution of the positioning system. The dark zones of the navigation unit cell correspond to nearly 10% of the covered area. The region confined to a narrower area is the α region, resultant from the irradiation pattern of three LEDs, followed by the central region (β) where the four LEDs contribute. Regions with poorer resolution are ε + ε' and Δ+ δ, assigned respectively, to optical signals from two and one LEDs.

B. Footprint characterization based on the LED propagation model

LEDs are modeled as Lambertian source where the luminance is distributed uniformly in all directions, whereas the luminous intensity is different in all directions. The luminous intensity for a Lambertian source is given by the following equation [24]:

$$I(\phi) = I_N \cos^m(\phi) \quad (10)$$

where *m* is the order derived from a Lambertian pattern, I_N is the maximum luminous intensity in the axial direction

and , ϕ is the angle of irradiance. The Lambertian order m is given by:

$$m = -\frac{\ln(2)}{\ln(\cos(\phi_{1/2}))} \quad (11)$$

As the half intensity angle ($\phi_{1/2}$) is of 60º, the Lambertian order m is 1.

The light signal is received by the WDM photodetector that detects the on/off states of the LEDs, generates a binary sequence of the received signals and convert data into the original format. For simplicity, we will consider a line of sight (LoS) connection for both VLC links, which corresponds to the existence of straight visibility between the transmitter and the receiver. In Figure 4 it is plotted the geometry of the transmitter and receiver relative position, with emphasis to the main parameters used for characterization of the LED source and the photodiode receiver (angles of irradiance and illumination, transmitter's semi-angle at half-power and field of view). The Lambertian model is used for LED light distribution and MatLab simulations are used to infer the signal coverage of the LED in the illuminated indoors space [25].

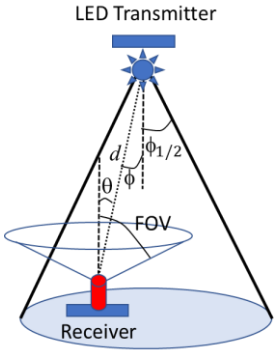

Figure 4. Transmitter and receiver relative position.

The link budget of the VLC link is evaluated computing the gains and losses along the propagation path of the light. It uses the channel gain of the link, which includes the losses due to the path and to wavelength in free space, as well as the spatial delivered power distribution by each emitter. The channel gain (G) is given by equation [26]:

$$G = \frac{(m+1)A}{2\pi D_{t-r}^2} I_N \cos^m(\phi) \cos(\theta) \quad (12)$$

where A is the area of the photodetector.

The evaluation of the channel gain allowed the establishment of the coverage map, that is illustrated in Figure 5. Only high accuracy footprints of the navigation cell are displayed. Each footprint region labelled as #1, #2, …, #9 are assigned to the correspondent optical excitation illustrated on the right side of Figure 5.

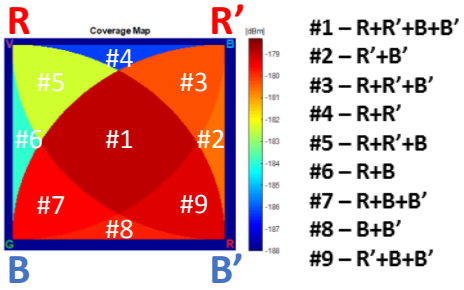

Figure 5. Coverage map of the fine-grain footprint inside the navigation cell, considering as VLC optical sources the top red and bottom blue emitters.

The use of the propagation model confirmed the theoretical prediction (Figure 3) and demonstrated the existence of distinct regions inside the navigation cell, that are assigned to the footprint [27], [28].

C. *Coding and modulation*

Data is converted into an intermediate data representation, byte format, and converted into light signals emitted by the VLC transmitter. The data bit stream is directed into a modulator that uses an ON–OFF Keying (OOK) modulation. Here, a bit assigned to one (1) is represented by an optical pulse that occupies the entire bit duration, while a bit set to zero (0) is represented by the absence of an optical pulse. The data format used to transmit information, namely, the length of the frame, the blocks that make part of the word in each frame and its contents must be known by the transmitter and receiver to ensure proper coding and decoding. In order to ensure synchronization between frames, two blocks labelled as Start of Text (SoT) and End of Text (EoT), are placed respectively, at the beginning and end of the word. The SoT is composed of two idle bits (logical value 1) and two start bits (logical value 0), which corresponds to the 4-bits word 1100. The EoT block is composed of two stop bits (logical value 0) and two idle bits (logical value 1), which corresponds to the 4-bits word 0011.

D. *Decoding strategy*

Based on the measured photocurrent signal by the photodetector, it is necessary to infer the correspondent footprint. For this purpose a calibration curve is previously defined in order to establish this assignment. In Figure 6 it is plotted the calibration curve that uses 16 distinct photocurrent thresholds resultant from the combination of the 4 modulated signals from the white VLC emitter. The driving current of each LED emitter was adjusted to provide different levels of photocurrent.

 ISBN: 978-1-61208-918-8

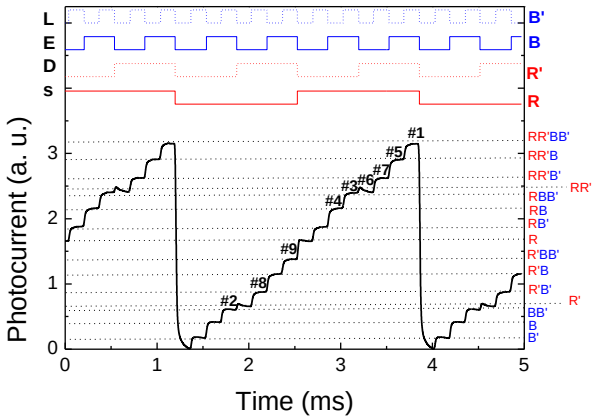

Figure 6. Calibration front photocurrent signal using two red and two blue optical signals modulated with multiple frequencies (on the top it is displayed the waveform of the emitters modulation state).

The correspondence between each footprint and the photocurrent level is highlighted on the right side of Figure 6. The correct use of this calibration curve demands a periodic retransmission of curve to ensure a accurate correspondence to the output signal and an accurate decoding of the transmitted information.

IV. RESULTS AND DISCUSSION

In Figure 7, it is displayed the photocurrent signal acquired by the mobile receiver unit at two different spatial positions inside the navigation cell covered by RR'BB' and R'BB' optical signals, which corresponds, respectively, to the footprints labelled as #1 and #9. The calibration curve is also displayed.

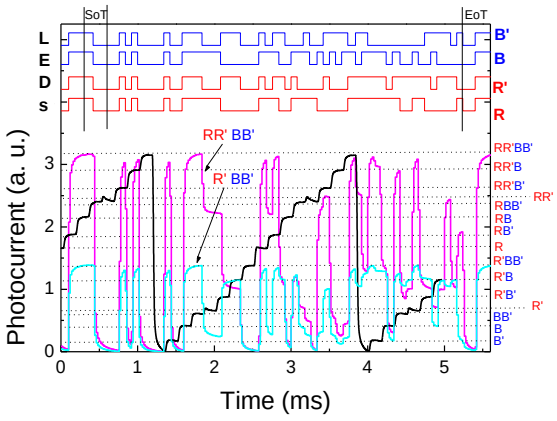

Figure 7. Photocurrent signal acquired by the mobile receiver unit at footprints #1 and #9 inside the navigation cell (RR'BB' and R'BB'). The calibration curve is also displayed.

Synchronization between frames is detected by the blocks SoT and EoT. In both measurements, either inside footprints #1 and #9 (RR'BB' and R'BB'), the presence of these blocks corresponds to maximum values of the photocurrent, because all emitters are simultaneously ON. The decoding of the photocurrent levels uses the calibration curve to identify which emitters are active in the duration period of each bit. On the right side of the graph it is stated the optical state assigned to each step of the calibration curve. The observed correspondence between the different thresholds of the measured signal and the steps of the calibration provide the decoding of the input optical signals.

V. CONCLUSIONS

In this paper, a VLC system for indoor navigation was presented. A theoretical study on the irradiation patterns is presented to support the position resolution of the proposed system and establish the footprint of each navigation cell. The optical signals transmitted by the RGB white LEDs were fully characterized using the Lambertian model. The footprint was predicted using the channel gain model of the transmitter-receiver link. Experimental results demonstrate the capability of the system. Future work will comprise a more detailed and complete description of the decoding methodology.

ACKNOWLEDGEMENTS

This work was sponsored by FCT – Fundação para a Ciência e a Tecnologia, within the Research Unit CTS – Center of Technology and systems, reference UID/EEA/00066/2019 and by project IPL/2020/Geo-Loc/ISEL.

REFERENCES

[1] R. Mautz, "Overview of Current Indoor Positioning Systems", Geodesy Cartogr., vol. 35, pp. 18–22, 2009.

[2] Y. Gu, A. Lo, and I. Niemegeers, "A Survey of Indoor Positioning Systems for Wireless Personal Networks," IEEE Commun. Surv. Tutor., vol. 11, pp. 13–32, 2009.

[3] A. M. Căilean and M. Dimian, "Current Challenges for Visible Light Communications Usage in Vehicle Applications: A Survey", IEEE Communications Surveys & Tutorials, vol. 19, no. 4, pp. 2681-2703, 2017.

[4] M. Z. Chowdhury, M. T. Hossan, A. Islam, and Y. M Jang, "A Comparative Survey of Optical Wireless Technologies: Architectures and Applications", IEEE Access, vol. 6, pp. 9819-9840, 2018.

[5] G. Cossu, A. M. Khalid, P. Choudhury, R. Corsini, and E. Ciaramella, "3.4 Gbit/s Visible Optical Wireless Transmission Based on RGB LED," Optics Express, vol. 20, pp. B501–B506, 2012.

[6] M. Kavehrad, "Sustainable Energy-Efficient Wireless Applications Using Light", IEEE Communications Magazine, vol. 48, no. 12, pp. 66-73, 2010.

[7] E. Ozgur, E. Dinc, and O. B. Akan, "Communicate to illuminate: State-of-the-art and research challenges for visible light communications", Physical Communication, vol. 17, pp. 72–85, 2015.

[8] C. Yang and H. R. Shao, "WiFi-based indoor positioning", IEEE Commun. Mag., vol. 53, no. 3, pp. 150–157, 2015.

[9] E. F. Schubert and J. K. Kim, "Solid-state light sources getting smart", Science, vol. 308, no. 5726, pp. 1274-1278, 2005.

 ISBN: 978-1-61208-918-8

[10] J.-Y. Sung, C.-W. Chow, and C.-H Yeh, “Is blue optical filters necessary in high speed phosphor-based white light LED visible light communications?”, Optics Express, vol. 22, no. 17, pp. 20646-20651, 2014.

[11] H. Le Minh et al, “High-speed visible light communications using multiple-resonant equalization,” IEEE Photon. Technol. Lett., vol. 20, no. 14, pp. 1243–1245, 2008.

[12] A. M. Khalid, G. Cossu, R. Corsini, P. Choudhury, and E. Ciaramella, “1-Gb/s transmission over a phosphorescent white LED by using rate-adaptive discrete multitone modulation”, IEEE Photon. J., vol. 4, no. 5, pp. 1465–1473, 2012.

[13] Z. Zhou, M. Kavehrad, and P. Deng, “Energy efficient lighting and communications”, Proc. SPIE 8282, Broadband Access Communication Technologies VI, vol. 8282, pp. 82820J-1-82820J-15, 2012.

[14] A. Jovicic, J. Li, and T. Richardson, “Visible Light Communication: Opportunities, Challenges and the Path to Market”, IEEE Communications Magazine, vol. 51, no. 12, pp. 26-32, 2013.

[15] P. Louro, et al, “Optical demultiplexer based on an a-SiC:H voltage controlled device”, Phys. Status Solidi C, vol. 7, no. 3–4, pp. 1188–1191, 2010.

[16] M. Vieira, M. A. Vieira, P. Louro, V. Silva, and P. Vieira, “Optical signal processing for indoor positioning using a-SiC:H technology”, Opt. Eng., vol 55, no. 10, pp. 107105-1-107105-6, 2016.

[17] M. A. Vieira, M. Vieira, P. Louro, and P. Vieira, "Cooperative vehicular communication systems based on visible light communication," Opt. Eng., vol. 57, no. 7, pp. 076101-, 2018.

[18] P. Louro; V. Silva; M. A. Vieira, and M. Vieira, “Viability of the use of an a-SiC:H multilayer device in a domestic VLC application”, Phys. Status Solidi C, vol, 11, no. 11–12, pp. 1703–1706, 2014.

[19] P. Louro, J. Costa, M. Vieira, M. A. Vieira, and Y. Vygranenko, “Use of VLC for indoors navigation with RGB LEDs and a-SiC:H photodetector”, Proc. of SPIE, Optical sensors, vol. 10231, pp. 102310F-1-102310F-10, 2017.

[20] P. Louro, J. Costa, M. A. Vieira, and M. Vieira, “Optical Communication Applications based on white LEDs”, J. Luminescence, vol. 191, pp. 122-125, 2017.

[21] M. Vieira, M. A. Vieira, I. Rodrigues, V. Silva, and P. Louro, “Photonic Amorphous Pi’n/pin SiC Optical Filter Under Controlled Near UV Irradiation”, Sensors & Transducers, vol. 184, no. 1, pp. 123-129, 2015.

[22] P. Louro, M. Vieira, and M. A. Vieira, “Indoors Geolocation Based on Visible Light Communication”, Sensors & Transducers, vol. 245, no. 6, pp. 57-64, 2020.

[23] P. Louro, M. Vieira, M. A. Vieira, and J. Costa, “Photodetection of modulated light of white RGB LEDs with a-SiC:H device”, Advanced Materials Proceedings, vol. 3, no. 5, pp. 366-371, 2018.

[24] Y. Zhu, W. Liang, J. Zhang, and Y. Zhang, “Space-Collaborative Constellation Designs for MIMO Indoor Visible Light Communications,” IEEE Photonics Technology Letters, vol. 27, no. 15, pp. 1667–1670, 2015.

[25] S. I. Raza, et al, ”Optical Wireless Channel Characterization For Indoor Visible Light Communications”, Indian Journal of Science and Technology, vol 8, no. 22, pp. 1 – 9, 2015.

[26] Y. Qiu, H.-H. Chen, and W.-X. Meng, “Channel modeling for visible light communications - a survey”, Wirel. Commun. and Mob. Comput., vol. 16, pp. 2016–2034, 2016.

[27] P. Louro, M. Vieira, and M. A. Vieira, "Bidirectional visible light communication," Opt. Eng., vol. 59, no. 12, pp. 127109-1, 127109-14, 2020.

[28] P. Louro, M. Vieira, P. Vieira, J. Rodrigues, and M. de Lima, "Geo-localization using indoor visible light communication", Proc. SPIE, Optical Sensors, vol. 11772, pp. 117720J-1-117720J-12, 2021.

 ISBN: 978-1-61208-918-8